PIER C

(Received 3 November 2025, Accepted 13 February 2026, Scheduled 17 March 2026)

Wearable UWB Antenna on Jeans Substrate for High-Speed 5G and IoT Devices

Amalraj Taksala Devapriya* and Savarimuthu Robinson

Department of Electronics and Communication Engineering
Mount Zion College of Engineering and Technology, Pudukkottai, Tamil Nadu, India

ABSTRACT: A flexible ultra-wideband antenna is presented using a denim (jeans) textile substrate for wearable 5G and Internet of Things (IoT) applications. The antenna employs a coplanar waveguide (CPW) feed with a rectangular defected ground structure (DGS) etched in the ground plane to improve impedance matching. Bandwidth enhancement is achieved by introducing a nested U-slot in the radiating patch. The proposed design operates over the 1.28–6 GHz frequency range, providing an impedance bandwidth of approximately 4.72 GHz. The measured realized gain varies from 2.1 to 5.3 dBi, while the simulated radiation efficiency remains above 80% across most of the operating band. Good agreement between simulated and measured results confirms stable radiation characteristics, demonstrating the suitability of the antenna for wearable ultra-wideband and sub-6 GHz communication systems.

1. INTRODUCTION

The rapid expansion of sub-6 GHz 5G wireless communication has driven significant research interest in compact, wideband, and efficient antennas for Internet of Things (IoT), Internet of Vehicles (IoV), and wearable applications [1]. Unlike conventional narrowband systems, sub-6 GHz platforms require antennas that offer wide impedance bandwidth, stable gain, low latency, lightweight structure, mechanical flexibility, and cost-effective implementation [2]. Wearable and textile-integrated antennas have emerged as promising candidates for next-generation wireless systems because of their ability to conform to the human body and integrate seamlessly into garments [3, 4]. However, achieving wideband performance on textile substrates remains challenging due to high dielectric losses, nonuniform thickness, and sensitivity to bending and environmental conditions, which can degrade impedance matching and radiation efficiency [5, 6]. Coplanar waveguide (CPW)-fed antennas are particularly attractive for wearable applications because they support single-sided metallization, simplify fabrication, and inherently provide wideband impedance characteristics [3, 7]. To further enhance bandwidth, techniques such as slotting and defected ground structures (DGSs) have been widely applied on rigid substrates [8, 9]. However, their effectiveness on low-cost textile materials, especially for continuous ultra-wideband (UWB) operation extending into low-frequency IoT/Low Power Wide Area Network (LPWAN) bands, has not been sufficiently explored. Motivated by these challenges, this work proposes a CPW-fed ultra-wideband textile antenna on a denim (jeans) substrate, incorporating nested U-slots in the radiating patch and a rectangular DGS in the ground plane. The objective is to realize continuous 1.28–6 GHz operation supporting both IoT/LPWAN and sub-6 GHz 5G bands, while maintaining flexibility, moderate gain, acceptable efficiency, and stable performance under bending conditions.

Despite significant progress in sub-6 GHz and UWB antenna design, several challenges remain when these solutions are adapted for wearable and textile-based applications. Most existing wideband antennas are implemented on rigid substrates, which limits conformability and integration into clothing. Designs targeting flexible platforms often focus on mid-band 5G frequencies and do not provide continuous coverage extending into lower IoT/LPWAN bands. In addition, many reported wearable antennas achieve bandwidth enhancement at the expense of reduced radiation efficiency, while essential considerations, such as bending robustness and human-body safety, are frequently underexplored. A detailed discussion of these limitations in existing designs is provided in Section 2.

Major contribution:

- A jeans-based CPW-fed textile antenna is proposed, which achieves continuous ultra-wideband operation from 1.28 to 6 GHz, supporting both IoT/LPWAN (sub-1.5 GHz) and 5G Frequency Range 1 (FR1) applications.
- Nested U-slots combined with a rectangular defected ground structure (DGS) are employed to enhance impedance matching and bandwidth on a flexible textile substrate.
- The proposed antenna demonstrates wide impedance bandwidth, stable moderate gain (3–5 dBi), and high radiation efficiency, while maintaining conformality, mechanical robustness, and low fabrication cost, making it suitable for wearable IoT devices, smart clothing, and sub-6 GHz 5G applications, as illustrated in Fig. 1.

* Corresponding author: Amalraj Taksala Devapriya (taksala@gmail.com).

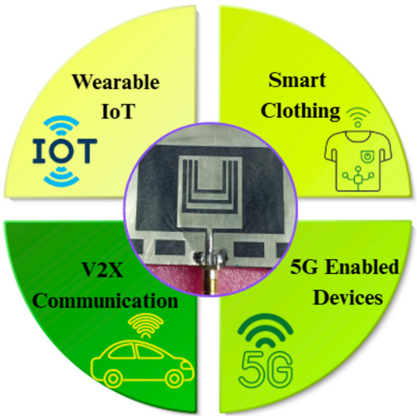

FIGURE 1. Application of the proposed wideband textile antenna.

2. RELATED WORK

A wide range of antenna designs have been reported for sub-6 GHz and UWB applications using various bandwidth-enhancement techniques, such as slotting [1, 2, 10, 11], fractal geometries [7], parasitic elements [10, 12, 13], metamaterials, frequency-selective surfaces (FSS) [3, 14, 15], and artificial magnetic conductors (AMC) [16, 17]. These approaches have demonstrated improved impedance bandwidth or gain; however, most are implemented on rigid substrates, such as FR-4, Rogers, or Arlon laminates, which limit conformability and restrict their use in wearable applications. Several studies focus primarily on the mid-band 5G spectrum (3.3–4.9 GHz) [2, 10, 12, 13, 18], providing limited or no coverage for lower-frequency IoT/LPWAN bands below 1.5 GHz. Designs that achieve wider bandwidths often rely on bulky multilayer structures, AMC/FSS reflectors, or array configurations [15–17], which are unsuitable for integration into clothing due to increased thickness, weight, and fabrication complexity.

Flexible antenna designs have been explored using polyimide substrates [3], demonstrating mechanical flexibility but at a relatively high material cost and limited compatibility with textile manufacturing processes. Textile-based antennas using denim, cotton, or polyester have been reported in a small number of studies [4, 5, 19]; however, these designs typically suffer from narrow bandwidth, reduced radiation efficiency, or lack systematic evaluation under bending and human-body loading conditions. Furthermore, although CPW-fed, slotting, and defected ground structure (DGS) techniques are individually well established on rigid substrates [8, 9, 20–24], including rectangular U-slot and DGS-based bandwidth enhancement approaches, their combined and optimized application on low-cost textile substrates has rarely been investigated.

Research Gaps Identified:

From the above review, the following gaps can be identified:

- Lack of textile-based antennas providing continuous ultra-wideband operation starting below 1.5 GHz.
- Limited use of low-cost, garment-compatible materials, such as denim, for wideband sub-6 GHz antennas.
- Insufficient exploration of combined CPW-fed, slotting, and DGS techniques on flexible substrates.
- Inadequate evaluation of wearable-specific factors, including bending stability and SAR compliance.

The present work addresses these gaps by proposing a CPW-fed denim textile antenna incorporating nested U-slots and a rectangular DGS, achieving continuous 1.28–6 GHz operation with stable gain, high efficiency, and verified wearable safety.

The antenna design equations and procedures are presented in Section 3. The operating principles and bandwidth-enhancement mechanisms are discussed in Section 4. A detailed parametric analysis is provided in Section 5, followed by simulated and measured results in Section 6. Finally, conclusions are drawn in Section 7.

3. ANTENNA DESIGN

The proposed antenna is designed on an ondenim (jeans) substrate using Equations (1)–(6) [8], as shown in Fig. 2(a). A nested U-slot configuration is introduced in the radiating patch, as illustrated in Fig. 2(b), to enhance the impedance bandwidth by creating multiple current paths. All geometric parameters of the antenna are listed in Table 1. The antenna is excited using a CPW feed that provides a good 50-Ω impedance match. To further improve impedance matching and radiation performance, a rectangular defected ground structure (DGS) is etched in the CPW ground plane, as shown in Fig. 2(c). The resulting design maintains a compact profile while achieving ultra-wideband operation, making it suitable for sub-6 GHz applications.

TABLE 1. Structural parameters of the proposed wideband textile antenna.

Parameter	Dimension (in mm)
Patch ($l_p \times W_p$)	25×22
Substrate ($l_s \times W_s$)	50×80
Outer slot ($l_1 \times W_1$)	30×50
Feed ($l_f \times w_f$)	14×1.6
CPW width	77.2
CPW feed gap (g_1)	0.6
Outer U slot ($h_1 \times t_1$)	18.5×1.5
Mid U slot ($h_2 \times t_2$)	15×1.2
Inner U slot ($h_3 \times t_3$)	11.5×1.2
Rectangular DGS ($d_2 \times d_1$)	5×10
Gap from CPW feed (g_2)	6.85
Gap between DGS (g_3)	4

The wavelength of the antenna can be calculated as,

$$\lambda = \frac{C}{f_r} \tag{1}$$

where C is the speed of light, and f_r is the resonant frequency. Using this value, the width of the patch (W) antenna can be

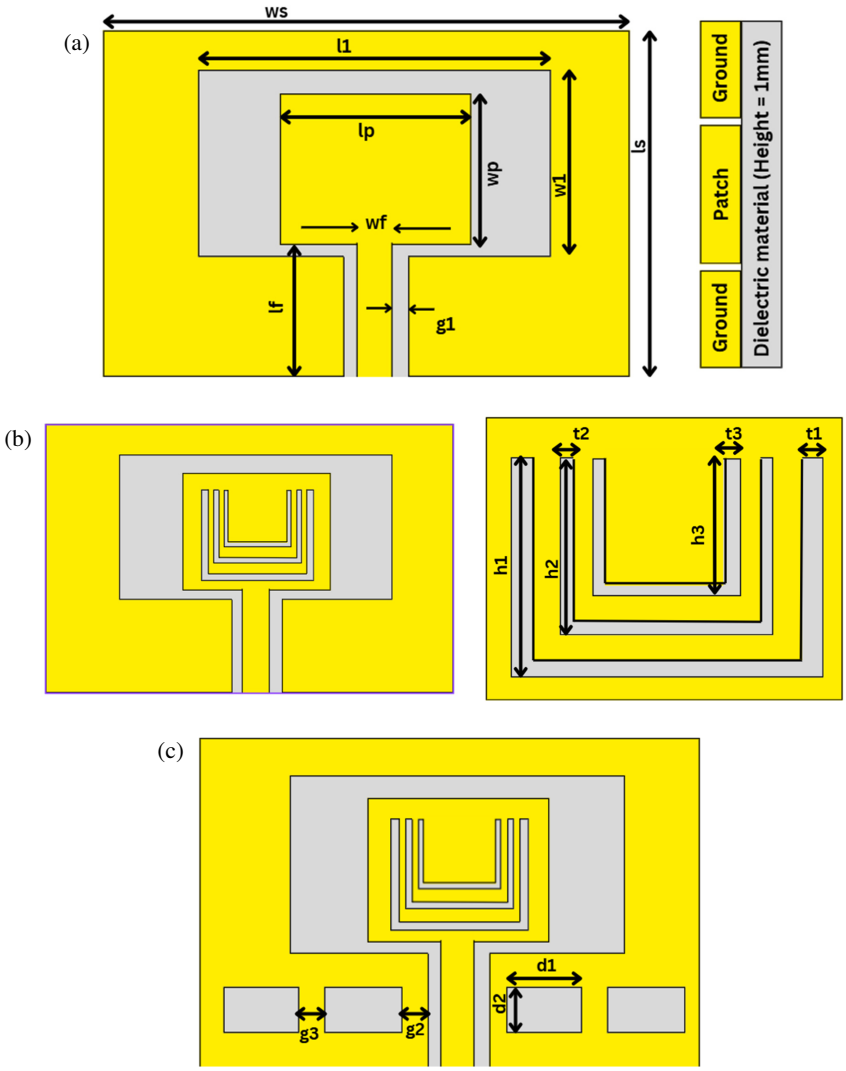

FIGURE 2. Antenna design steps: (a) CPW-fed patch, (b) nested U-slot, and (c) final configuration with DGS.

calculated as,

$$W_p = \frac{C}{2f_r}\sqrt{\frac{2}{1+\varepsilon_r}} \tag{2}$$

where ε_r is the relative permittivity (dielectric constant). From this, the effective permittivity ε_{eff} can be calculated as

$$\varepsilon_{eff} = \frac{\varepsilon_r + 1}{2} + \frac{\varepsilon_r - 1}{2}\left(1 + 12\frac{h}{W}\right)^{-\frac{1}{2}} \tag{3}$$

where h is the thickness of the substrate. Furthermore, the length of the patch (L) can be expressed as,

$$L_p = \frac{C}{2f_r\sqrt{\varepsilon_{eff}}} - 0.824\,\frac{\left(\frac{W}{h} + 0.264\right)\left(\varepsilon_{eff} + 0.3\right)}{\left(\frac{W}{h} + 0.8\right)\left(\varepsilon_{eff} - 0.258\right)}\,h \tag{4}$$

Finally, the width (W_s) and length (L_s) of the substrate are defined as

$$W_s = W_p + (6 * h) \tag{5}$$

$$L_s = L_p + (6 * h) \tag{6}$$

4. ANTENNA OPERATION AND BANDWIDTH ENHANCEMENT MECHANISMS

The proposed antenna achieves ultra-wideband (UWB) performance over the 1.28–6 GHz frequency range by combining three key structural features:

- Coplanar waveguide (CPW) feed,
- Nested U-slots in the radiating patch, and
- Rectangular defected ground structure (DGS) slots introduced in the CPW ground wings.

Each feature plays a distinct role in achieving broadband impedance matching and stable radiation characteristics.

4.1. Coplanar Waveguide (CPW) Feed

The CPW feed is employed to excite the radiating patch due to its inherent wideband impedance characteristics, ease of integration, and single-sided metallization [3, 7], which are particularly advantageous for textile fabrication [4]. Unlike conventional microstrip feeds, the CPW configuration enables effec-

TABLE 2. Functional parameters of CPW-fed antenna at each step.

Parameters	Step 1 with CPW-Fed	Step 2 with nested U slot	Step 3 with DGS
Resonant frequency (GHz)	3, 4.2	3.2, 4.05	2.5, 3.05, 4.05
Reflection Coefficient (dB)	−34.84, −15.33	−14.15, −13.33	−21.65, −28.45, −24.52
Gain (dB)	3.77, 1.23	4.38, 3.79	2.66, 3.32, 2.99
Radiation Efficiency (%)	99.68, 98.79	97.27, 96.49	98.89, 98.49, 97.08
Bandwidth Spectrum	2.5–3.5, 3.95–4.3	2.55–4.2	1.23–6
Bandwidth (GHz)	1, 0.35	1.65	4.77
Fractional Bandwidth (%)	33%, 8.48%	24.44%	129%
SAR (W/Kg)	-	-	1.43

tive control of the surface current distribution, thereby reducing the effective characteristic impedance and naturally supporting broadband matching [5]. In addition, CPW feeding suppresses substrate surface-wave losses and improves radiation efficiency, which is especially beneficial for low-permittivity textile substrates, such as denim ($\varepsilon_r \approx 1.7$) [6].

4.2. Nested U-Slots in the Patch

The radiating patch incorporates multiple nested U-shaped slots of different lengths, similar to multiband U-slot techniques reported in [25–27]. Each U-slot introduces an additional current path corresponding to a distinct quarter-wavelength resonance. The outer U-slot supports lower-frequency resonances by extending the effective current path, while the inner slots excite higher-order resonances [19, 26, 27]. The overlap of these resonances produces a continuous wideband response covering 1.28–6 GHz. Moreover, the nested slot configuration smooths impedance variations, resulting in a stable S_{11} response across the entire operating band. This behavior is consistent with previously reported bandwidth-enhancement mechanisms for both rigid substrates and wearable textile antennas incorporating DGS [19, 28].

4.3. Rectangular Slots in the CPW Ground Wings (Defected Ground Structure)

Rectangular slots are etched in the CPW ground plane near the feedline, forming a defected ground structure that perturbs the surface current distribution and introduces additional parallel resonant modes [9, 20, 21]. These DGS elements effectively increase the inductance and capacitance of the ground region, thereby lowering the cut-off frequency and extending antenna operation toward the lower IoT/LPWAN band (around 1.28 GHz), as reported in earlier DGS-enhanced CPW antenna studies [9, 20]. At the same time, the DGS improves impedance matching at mid- and high-frequency regions by suppressing undesired surface-wave modes and redistributing ground currents [25]. When combined with CPW-fed slot-based designs [29–31], this approach enables compact broadband antennas with smooth S_{11} characteristics and stable radiation patterns.

4.3.1. Combined Effect

The CPW feed provides inherent broadband excitation and compatibility with textile substrates. The nested U-slots generate multiple resonances that overlap to produce ultra-wideband coverage, while the rectangular DGS in the CPW ground wings further tunes the impedance profile, lowers the operating frequency, and stabilizes radiation characteristics. Together, these features enable continuous 1.28–6 GHz operation with stable moderate gain (3–5 dBi) and high radiation efficiency, overcoming the narrowband limitations of conventional textile microstrip antennas.

Figure 3 presents a comparative performance analysis of the antenna evolution across the three design steps, including reflection coefficient (S_{11}), gain, and efficiency. As shown in Fig. 3(a), Step 1 exhibits limited impedance bandwidth with shallow resonances, while Step 2 improves matching but remains narrowband. The final configuration (Step 3) achieves significant enhancement, with S_{11} remaining below -10 dB over the wide frequency range of 1.28–6 GHz, confirming the effectiveness of the slotting and ground modifications. The corresponding gain characteristics in Fig. 3(b) show that Step 3 maintains higher and more stable gain across the operating band, with minor fluctuations at higher frequencies due to higher-order mode excitation. Fig. 3(c) illustrates the radiation efficiency of the final design, which remains consistently high across the band. The variation of S_{11} under bending conditions is presented in Fig. 3(d), indicating stable impedance performance during deformation. To evaluate dielectric perturbation effects under bending, the substrate permittivity is varied under the bending radius of 20 mm. As shown in Fig. 3(e), the maximum resonance shift is observed as 5%, while the impedance bandwidth remains nearly unchanged when ε_r is varied from 1.65 to 1.75. All functional parameters are summarized in Table 2. The resonant behavior of the antenna is modeled using a parallel RLC circuit, which captures both the resistive and reactive components of the input impedance.

The simulated input impedance (Z_{in}) was exported, and each resonance was approximated by a parallel RLC branch. The three branches correspond to the fundamental CPW-patch mode ($R1$-$L1$-$C1$), the additional mode introduced by the nested U-

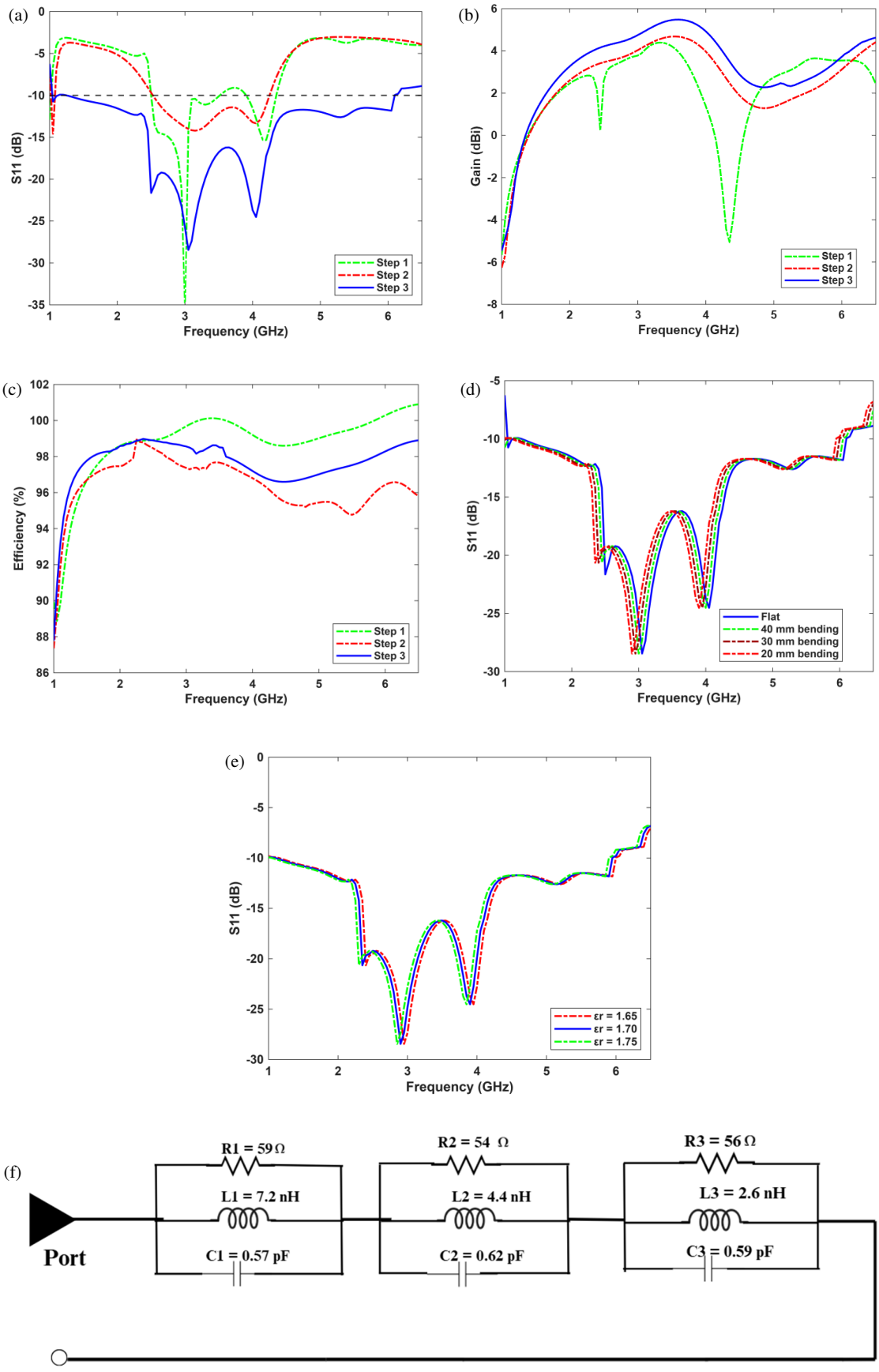

FIGURE 3. Performance at each design step: (a) S_{11}, (b) gain, (c) efficiency, (d) S_{11} under bending, (e) effect of dielectric perturbation under bending and (f) equivalent circuit.

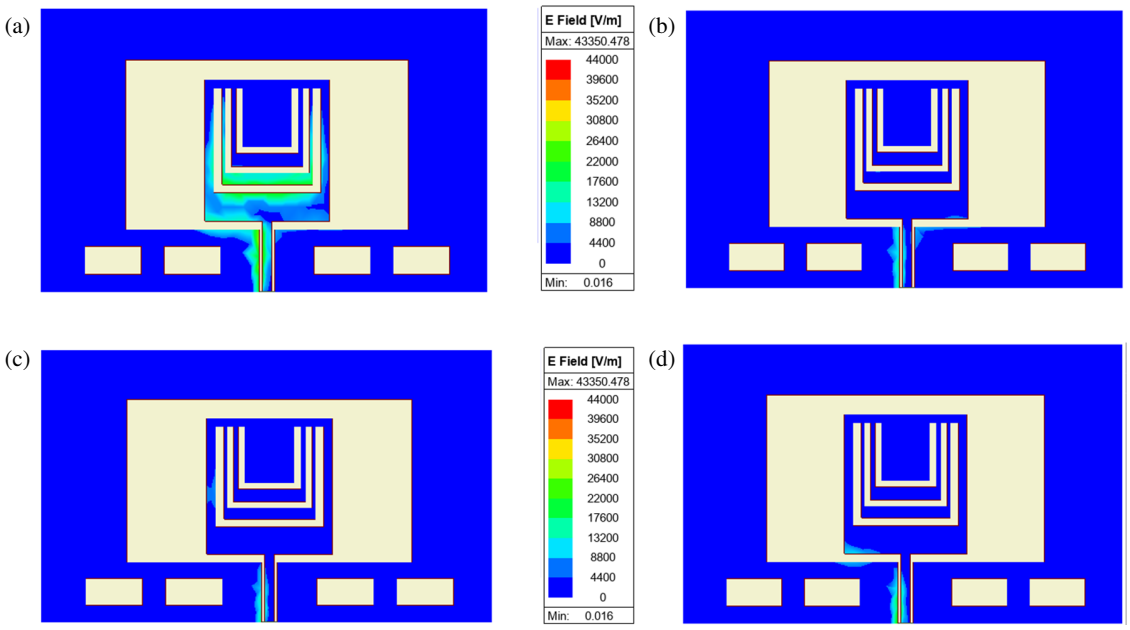

FIGURE 4. (a) Surface current distribution at 2.4 GHz, (b) at 3 GHz, (c) at 4 GHz, and (d) at 6 GHz.

slot ($R2$-$L2$-$C2$), and the resonance associated with the DGS in the CPW ground ($R3$-$L3$-$C3$). Initial values of L and C were estimated from the resonant frequencies, while the real part of the input impedance at resonance was taken as the resistance. The quality factor (Q), input impedance, and equivalent inductance and capacitance values were calculated using the equations in [15].

$$Q = \frac{f_r}{BW} \tag{7}$$

where Q is the quality factor, and bandwidth (BW) is the resonance bandwidth.

$$\omega_0 = 2\pi f_r \tag{8}$$

where ω_0 is the angular frequency of resonance.

$$Z_{in} = R = Z_0 \frac{1+\Gamma_0}{1-\Gamma_0} \tag{9}$$

where Z_{in} is the input impedance, Z_0 the characteristics impedance, and Γ_0 the reflection coefficient.

$$L = \frac{R}{\omega_0 Q} \quad \text{and} \quad C = \frac{Q}{R \cdot \omega_0} \tag{10}$$

where R is the resistance, L the inductance, and C the capacitance.

The equivalent circuit of the proposed antenna is shown in Figure 3(f).

Figure 4 shows the simulated surface current distribution of the proposed jeans-based CPW-fed antenna at representative frequencies of (a) 2.4 GHz, (b) 3 GHz, (c) 4 GHz, and (d) 6 GHz. At 2.4 GHz, strong current concentration is observed around the feed line and the inner U-slot, indicating the fundamental resonance. At 3 GHz, the current spreads across the nested U-slots, supporting the excitation of an additional resonant mode. At 4 GHz, multiple slots are activated with significant current density along the outer edges of the patch, confirming the role of slotting in bandwidth enhancement. At 6 GHz, the current distribution becomes more complex and is concentrated along the edges of the patch and ground slots, corresponding to higher-order modes. These results demonstrate that the combined effect of nested U-slots and the defected ground structure enables multiple resonances, leading to ultra-wideband operation.

5. PARAMETRIC STUDY

To systematically understand and optimize the proposed textile CPW-fed wideband antenna with nested U-slots, a focused parametric study was conducted on the substrate material and four key geometric parameters that strongly influence resonance behavior, impedance matching, and radiation performance. The parameters considered in this study are

- substrate material
- outer patch length (l_1),
- patch width (w_1)
- CPW-to-patch gap (g_1), and
- inter-DGS slot spacing (g_3).

Figure 5(a) presents the simulated reflection coefficient (S_{11}) of the antenna when it is implemented on three different textile substrates: cotton, denim (jeans), and polyester. The corresponding performance variations are summarized in Table 3. All three substrates support wideband impedance matching over the 1.28–6 GHz range with S_{11} below -10 dB. Cotton and polyester exhibit slightly improved matching near the 2.9 GHz resonance, whereas denim provides more stable impedance behavior at higher frequencies. Multiple resonances consistently

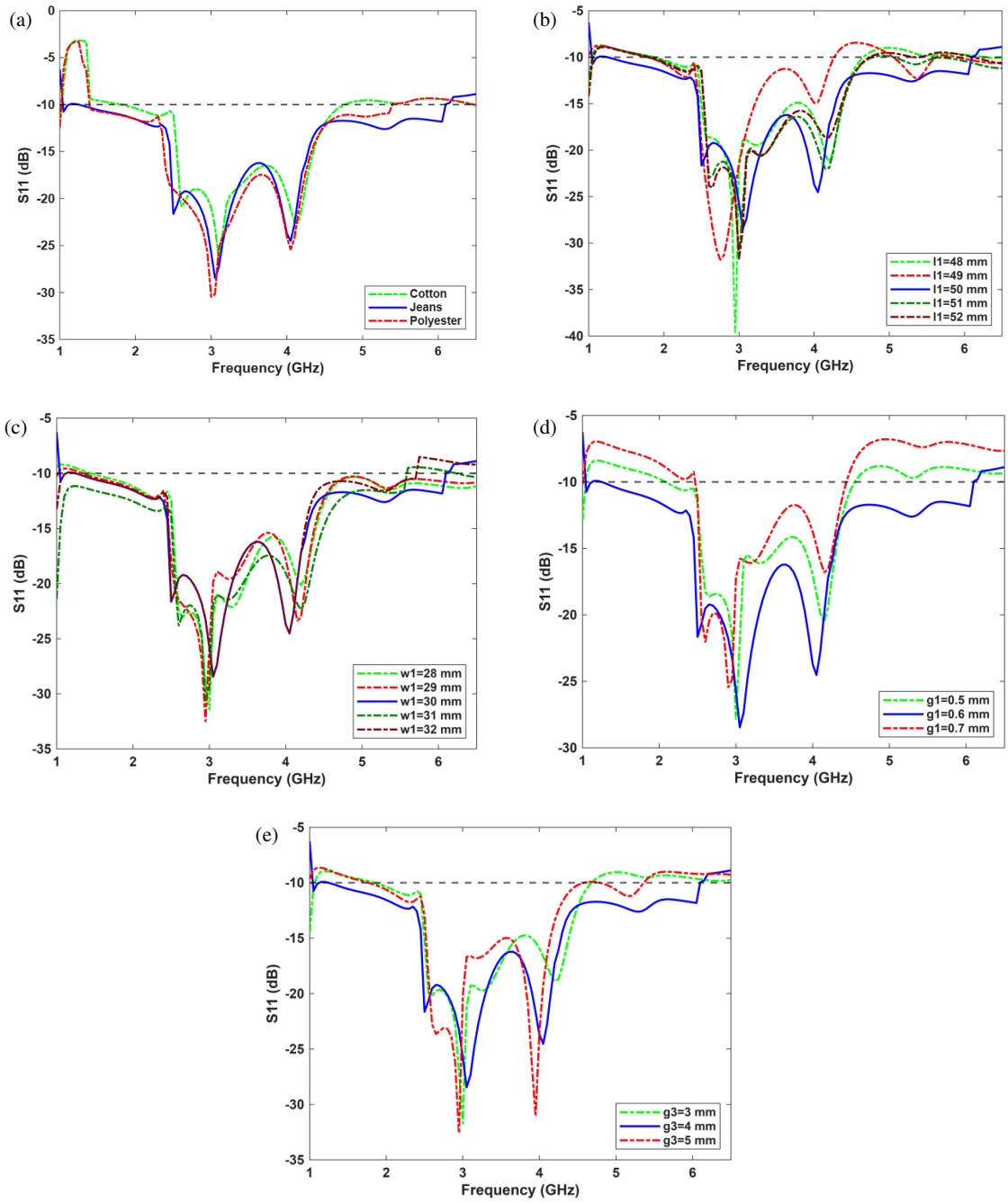

FIGURE 5. Parametric results: (a) S_{11} for different substrates, (b) effect of patch length L_1, (c) patch width W_1, (d) CPW-to-patch gap g_1, and (e) inter-slot spacing g_3.

TABLE 3. Impact of varying substrate material on the performance of the proposed antenna.

Parameters	Resonant frequency (GHz)	S_{11} (dB)	Bandwidth (GHz)
$\varepsilon_r = 1.6$ (Cotton)	2.6, 3.1, 4.15	$-20.80, -26.42, -22.55$	1.85–4.75
$\varepsilon_r = 1.7$ (Jeans)	2.5, 3.05, 4.05	$-21.65, -28.45, -24.52$	1.23–6
$\varepsilon_r = 1.9$ (Polyester)	3, 4.05,	$-30.44, -25.42$	1.4–5.35

appear around 2.5 GHz, 3.05 GHz, and 4.05 GHz, confirming the robustness of the design with respect to substrate permittivity. Although small frequency shifts occur due to variations in dielectric constant, the overall bandwidth remains largely unaffected. Denim is therefore preferred owing to its durability and suitability for wearable applications. Fig. 5(b) illustrates the effect of varying the outer slot length l_1 from 48 to 52 mm. This parameter strongly influences resonance tuning and impedance

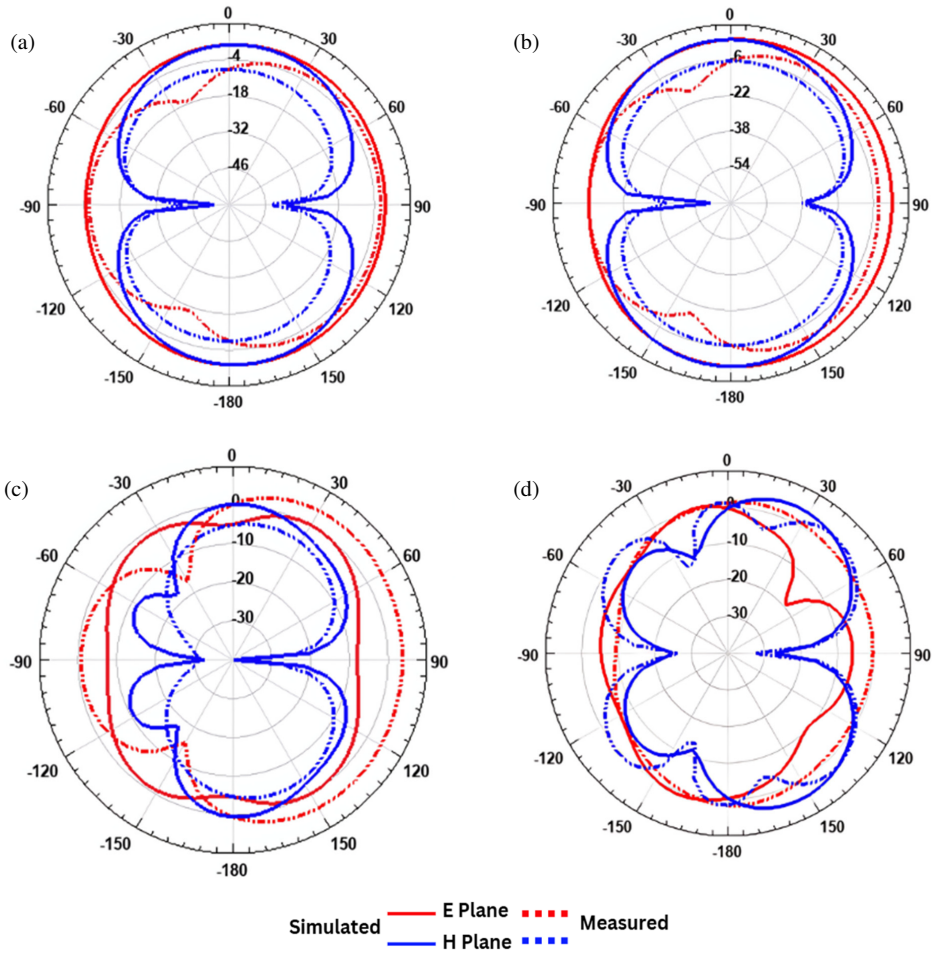

FIGURE 6. (a) Radiation pattern at 2.4 GHz, (b) at 3 GHz, (c) at 4 GHz, and (d) at 6 GHz.

matching. For $l_1 = 48$ mm and 49 mm, deeper notches are observed near 3 GHz; however, the high-frequency bandwidth is reduced. The optimal value, $l_1 = 50$ mm, results in well-distributed resonances covering the 1.23–6 GHz band with stable S_{11} below -10 dB.

Further increases in l_1 to 51 mm and 52 mm shift the resonances toward lower frequencies and degrade impedance matching at higher frequencies. The influence of patch width w_1 is shown in Fig. 5(c). While all configurations maintain wideband operation between 1.3 and 6 GHz, the resonance locations and impedance matching are sensitive to w_1. Smaller values (28–29 mm) produce a stronger resonance near 3 GHz but introduce ripples and mismatches above 5 GHz.

Increasing w_1 beyond 31 mm shifts the resonances downward and reduces high-frequency matching. Optimal performance is achieved at $w_1 = 30$ mm, where S_{11} remains consistently below -10 dB across the operating band. This behavior is attributed to the effect of w_1 on lateral current distribution and CPW-to-patch coupling, with an intermediate width providing the best compromise between resonance tuning and bandwidth stability. Fig. 5(d) shows the effect of varying the CPW-to-patch gap g_1, which controls the coupling strength between the feed and the radiating patch. At $g_1 = 0.5$ mm, strong resonances occur near 2.9 GHz and 4 GHz, but impedance matching degrades at higher frequencies. At $g_1 = 0.7$ mm, the resonances shift upward, and matching deteriorates below 3 GHz. The optimal gap, $g_1 = 0.6$ mm, offers the best balance, providing deep resonances, evenly distributed notches, and continuous wideband coverage from 1.28 to 6 GHz. Finally, Fig. 5(e) illustrates the influence of inter-DGS slot spacing g_3, varied from 3 to 5 mm. A smaller gap increases capacitive coupling and improves low-frequency resonance but limits high-frequency matching. Conversely, a larger gap weakens coupling, shifting resonances toward higher frequencies. At $g_3 = 3$ mm, good matching is observed near 2.9 GHz, but performance deteriorates above 4.5 GHz. At $g_3 = 5$ mm, low-frequency matching degrades, although stronger resonances appear near 3 GHz and 4 GHz. The optimal spacing, $g_3 = 4$ mm, provides the most stable ultra-wideband response, maintaining multiple resonances across the 1.28–6 GHz band with S_{11} consistently below -10 dB.

6. SIMULATED/MEASURED RESULTS AND DISCUSSION

After validating the antenna performance through full-wave simulations, experimental measurements were conducted on a fabricated prototype to verify agreement under realistic textile

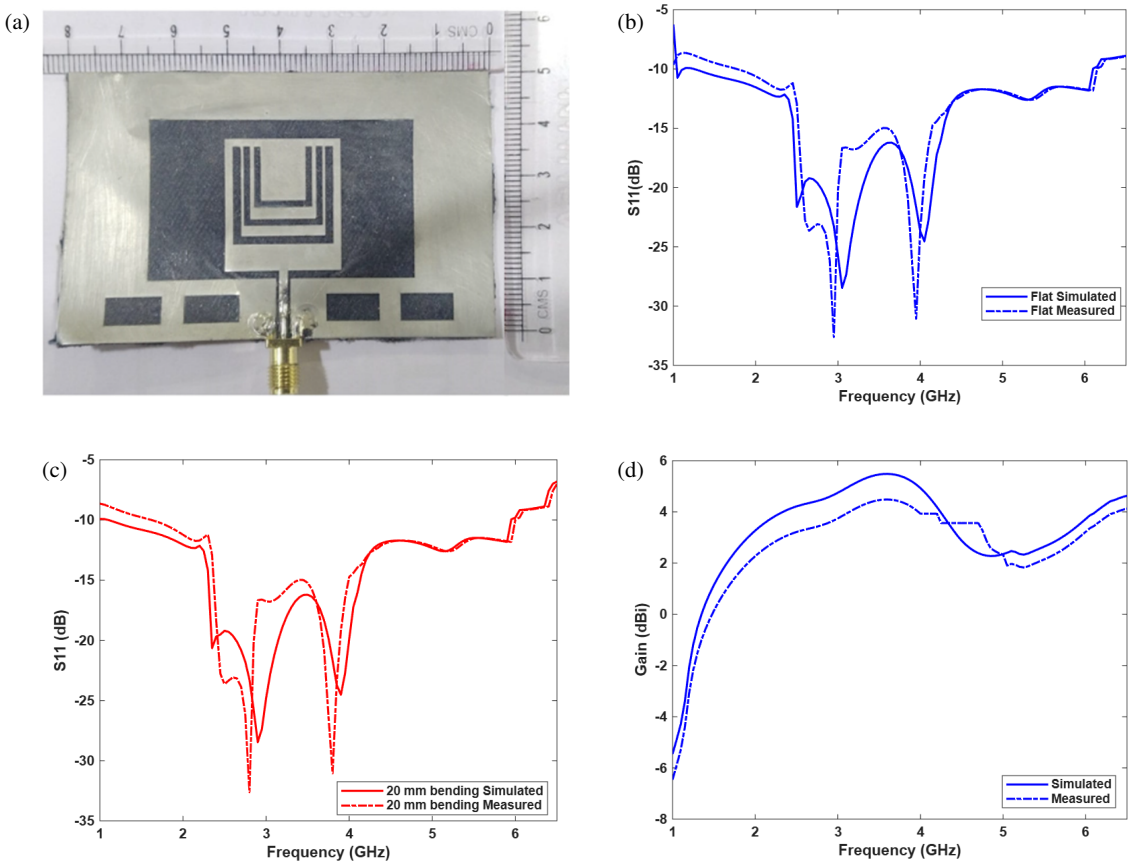

FIGURE 7. Prototype results: (a) fabricated antenna, (b) simulated/measured S_{11}, (c) S_{11} under 20 mm bending, and (d) gain comparison.

TABLE 4. Dielectric characteristics of human phantom model.

Tissue Layer	Relative Permittivity	Conductivity (S/m)	Mass Density (kg/m^3)	Thickness (mm)
Skin	38.09	1.43	1001	2
Fat	5.29	0.10	900	8
Muscle	52.82	1.69	1006	20
Bone	11.4	0.39	1008	13

conditions. This section compares simulated and measured results in terms of S_{11}, realized gain, radiation patterns, and bending performance. Fig. 6 shows the fabricated prototype and the corresponding measurement results. The antenna was implemented on a flexible textile substrate using conductive fabric for the radiating element and feed, as shown in Fig. 6(a). The prototype retained good mechanical flexibility and structural integrity, confirming its suitability for wearable environments.

Figure 6(b) compares the simulated and measured S_{11} responses under flat conditions. The measured results closely follow the simulated trends, validating the accuracy of the design and fabrication processes. Minor frequency deviations (less than 5%) are observed, which can be attributed to fabrication tolerances, connector losses, and variations in the dielectric properties of the textile substrate under ambient conditions. Distinct resonances are observed near 1.77 GHz, 3.75 GHz, 4.43 GHz, and 5.25 GHz, confirming the intended wideband operation.

The bending performance is illustrated in Fig. 6(c), where the antenna is wrapped over a cylindrical surface with a radius of 20 mm. The antenna maintains good impedance matching under bending, with slight upward shifts in resonant frequencies due to mechanical deformation and changes in surface current distribution. Nevertheless, all resonant bands remain within the targeted sub-6 GHz range, demonstrating mechanical robustness and suitability for conformal wearable deployment. A comparison of simulated and measured realized gains is presented in Fig. 6(d). The measured gain agrees well with simulation, remaining above 3 dBi across the operating band. Small discrepancies at higher frequencies are mainly attributed to measurement setup imperfections and connector alignment. Overall, the antenna exhibits stable gain character-

TABLE 5. Comparison of various wideband antennas with the proposed antenna.

Ref.	Antenna Type/Technique	Material	Size (mm^3)	Bandwidth (GHz)	Peak Gain (dBi)	Key Limitations
[1]	Circular patch with slots, and DGS	FR-4 ($\varepsilon_r = 4.4$)	$24 \times 30 \times 1.6$	1.5	0.2–6.1	VSWR up to 3.5, ground plane dependent, no prototype
[2]	Filtering patch, circular slot, T-shaped ground	FR-4 ($\varepsilon_r = 4.33$, $h = 0.8$)	$29 \times 35 \times 0.8$	1.8	3	Modest gain, FR4 losses, moderate suppression
[3]	Flexible UWB CPW + CSRR ground	Polyimide ($\varepsilon_r = 3.5$)	$23.885 \times 23.885 \times 1.405$	7.5	2.5–4.8	SAR not studied, durability untested
[5]	Half-circular spike monopole, CPW-fed	Jeans, cotton, silk	$60 \times 60 \times 1$	8.5	9.5	Focused on higher UWB; no support for IoT/LPWAN; no slotting or DGS for tuning
[7]	Dragon fractal CPW-fed	FR-4 ($\varepsilon_r = 4.4$)	$50 \times 45 \times 1.6$	3.03	5.5	No flexibility test, moderate gain
[10]	Circular patch + ground slot	FR-4 ($\varepsilon_r = 4.6$, $h = 1.6$)	$20 \times 28 \times 1.6$	2.77	4.2	FR-4 loss, slight pattern distortion at high freq.
[11]	Reconfigurable patch + DGS + PIN diodes	FR-4 ($\varepsilon_r = 4.2$)	$25 \times 28 \times 1.57$	6.4	1.6–5.8	Complex bias circuit, rigid, modest gain
[12]	Conformal patch + parasitic strips	Rogers RT5880 ($\varepsilon_r = 2.2$)	$73.10 \times 60.20 \times 0.787$	1	3.3 (single), 6.6 (array)	Band $< 30\%$, large element size
[13]	Inset-fed patch + parasitics	Rogers RT5880 ($\varepsilon_r = 2.2$)	$40 \times 40 \times 1.575$	1.5	2.5–3.5	Upper band < 4.2 GHz, rigid substrate
[14]	Rectangular patch + SRR metamaterial	FR-4 ($\varepsilon_r = 4.2$, $h = 1.6$)	$30 \times 25 \times 1.6$	0.46, 8.3	2.2	Sim. only, modest gain
[15]	1×4 patch array + FSS reflector	FR-4 ($\varepsilon_r = 4.4$, $h = 1.6$)	$136 \times 55 \times 1.6$	2.3	11.4–12.4	Very large size, complex air-gap structure
[17]	UWB MIMO + DGS + NL + AMC walls	FR-4 ($\varepsilon_r = 4.4$, $h = 1.55$)	$46 \times 46 \times 1.6$	2.55	6–9	"EL" slot into the radiating element and two identical stubs needed
[18]	Rectangular patch	Arlon ($\varepsilon_r = 2.98$)	$55.56 \times 52.92 \times 0.79$	0.120	7.5	Narrowband, rigid, no IoT/LPWAN coverage
[19]	Textile patch with C-slot, CPW	Denim, cotton, polyester	$18 \times 19 \times 1$	7.7	3–5	No operation below 3 GHz (IoT); slot shape different (C-slot, not U-slot);
[25]	Flower-shaped UWB MIMO + CSRR + U-slot	RT Duroid 5880 ($\varepsilon_r = 2.2$)	$30.5 \times 42.2 \times 0.79$	10.9	–	Gain not detailed, rigid, costly
This work	**Jeans-based CPW-fed + rectangular DGS + nested U-slot**	**Jeans textile ($\varepsilon_r \approx 1.6$, $h = 1$)**	$\mathbf{25.0 \times 22.0 \times 1.0}$	**Wide bandwidth (4.7 GHz)**	**3–5**	Textile washing effects need study

istics and consistent radiation efficiency, even under bending conditions.

Figure 7 illustrates the simulated and measured radiation patterns of the proposed antenna at four representative frequencies, namely 2.4 GHz, 3 GHz, 4 GHz, and 6 GHz. At 2.4 and 3 GHz, the antenna exhibits nearly omnidirectional characteristics in the H-plane with bidirectional patterns in the E-plane, resembling that of a monopole radiator. As the frequency increased to 4 GHz, slight distortions were observed in the radiation lobes owing to the excitation of higher-order modes; however, the overall symmetry was preserved. At 6 GHz, multiple radiation lobes and nulls appear, which is a typical behaviour of ultra-wideband antennas operating at higher resonances. Despite these variations, the antenna maintains a stable radiation performance across the band, confirming its suitability for sub-6 GHz wireless communication applications.

Specific absorption rate (SAR) evaluation was carried out using full-wave simulations with a multilayer human tissue phan-

tom comprising skin, fat, muscle, and bone layers, with dielectric and conductivity properties listed in Table 4. The antenna was placed directly on the phantom, and SAR was computed according to the IEEE C95.1 standard using 1 g spatial averaging. The simulated peak 1 g SAR value is 1.43 W/kg at an input power of 1 W as shown in Fig. 8, which is well below the Federal Communications Commission (FCC) safety limit of 1.6 W/kg.

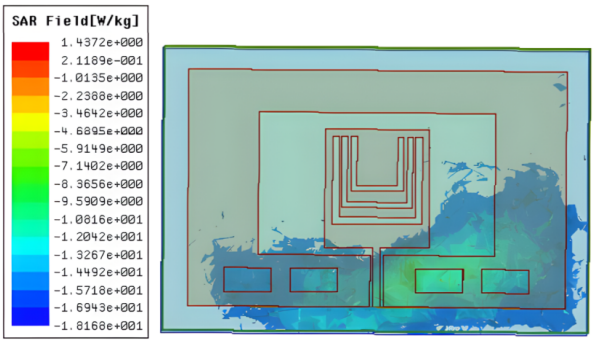

FIGURE 8. SAR of the proposed antenna.

A comparative evaluation of recently reported antennas for sub-6 GHz and UWB applications is presented in Table 5. Existing designs employ enhancement techniques, such as fractal geometries [3], parasitic elements [4, 6], filtering slots [2, 5], metamaterials [7, 9, 31], artificial magnetic conductor (AMC)/frequency selective surface (FSS) reflectors [8, 13, 14], and stepped-impedance resonators (SIR) [31]. While these approaches improve bandwidth or gain, most are implemented on rigid substrates, such as FR-4, Rogers, or Arlon [2–8, 12–14], which limits their applicability to wearable or conformal systems. Only a few flexible designs have been reported, notably polyimide-based structures [9], which remain costly and have not been extended to low-cost textile substrates.

In terms of bandwidth, many reported antennas focus on the mid-band 5G spectrum (3.3–4.9 GHz) [2, 10, 12, 13, 18]. Some designs extend further, such as the dragon fractal antenna in [7] (3.67–6.7 GHz) and metamaterial/AMC-based structures [13, 16, 17], which achieve wide or ultra-wide coverage. However, continuous wideband operation starting near 1.2 GHz required to simultaneously support IoT/LPWAN and 5G services — has rarely been addressed. The proposed textile antenna uniquely achieves continuous coverage from 1.28 to 6 GHz, effectively bridging this gap. With respect to gain performance, high-gain solutions, such as FSS-backed arrays [15], can achieve gains up to 12.4 dBi but require large and bulky structures unsuitable for wearable systems. In contrast, compact single-element antennas [2, 10, 13] and metamaterial-based designs [3, 14] typically provide moderate gains in the range of 2–5 dBi. The proposed antenna achieves a stable gain between 3 and 5 dBi with radiation efficiency above 80%, offering a practical trade-off among bandwidth, gain, and compactness. Finally, practical integration aspects are noteworthy. Most rigid FR-4 and Rogers-based antennas [2, 9, 10, 12–18] are intended for vehicular, base-station, or fixed IoT devices.

In contrast, the proposed antenna is implemented on a jeans textile substrate, providing a low-cost, flexible, and conformal solution suitable for wearable IoT and 5G applications. While textile materials may be affected by moisture absorption, stretching, surface roughness, and long-term aging, these factors represent opportunities for future improvement. Moreover, higher gain configurations or array implementations may be required for long-range communication, and the integration of sensing or energy modules will be essential for fully practical wearable IoT systems.

7. CONCLUSION

This work presents a flexible ultra-wideband antenna implemented on a denim (jeans) textile substrate for wearable 5G and Internet of Things (IoT) applications. From a theoretical perspective, the results demonstrate that a coplanar waveguide (CPW)-fed structure incorporating nested U-slots in the radiating patch and a rectangular defected ground structure (DGS) in the ground plane can effectively achieve a wide impedance bandwidth on a low-permittivity, lossy textile substrate. The proposed configuration confirms that appropriate slot-ground interaction enables continuous ultra-wideband behavior without compromising radiation performance.

The research contributions of this study are summarized as follows. A low-cost, flexible textile antenna capable of operating continuously from 1.28 to 6 GHz was developed, supporting both IoT/LPWAN and sub-6 GHz 5G frequency bands. The combined use of nested U-slots and a rectangular DGS within a CPW-feed configuration was shown to be an effective bandwidth-enhancement strategy on denim substrates. The antenna exhibits a stable realized gain in the range of 3–5 dBi, acceptable radiation efficiency, and compliance with SAR safety limits, confirming its suitability for wearable communication systems.

From a practical standpoint, the proposed antenna offers clear advantages for wearable deployment. The denim substrate enables seamless integration into garments while maintaining mechanical flexibility and low fabrication cost. The single-layer CPW-fed design avoids vias and multilayer structures, simplifying fabrication and improving robustness. In addition, the antenna maintains stable impedance matching and radiation characteristics under bending, making it suitable for smart wearables, IoT-connected garments, and body-mounted sub-6 GHz communication devices.

Nevertheless, some limitations remain. Textile materials are sensitive to environmental factors, such as moisture absorption, repeated bending, surface roughness, and long-term aging, which may influence antenna performance in prolonged use. Moreover, the single-element configuration limits the achievable gain compared with array-based or AMC-assisted designs, restricting its applicability in long-range communication scenarios.

Future research may build upon this work in several directions. First, textile-based multiple-input multiple-output (MIMO) or array configurations can be investigated to enhance gain, isolation, and link reliability while preserving flexibility. Second, long-term durability studies, including washing,

humidity, sweat exposure, and mechanical fatigue, should be conducted to assess performance stability in realistic wearable conditions. Third, integration with sensing modules or energy-harvesting units may enable fully self-contained wearable IoT platforms for next-generation smart clothing applications.

REFERENCES

[1] Kalyani, G., D. G. S. Rao, K. Sravani, N. Sirisha, and B. Mahathi, "Design of a wide band circular patch antenna for WiMAX, C-band and 5G sub-6 GHz communication application," *International Journal of Research and Review*, Vol. 12, No. 5, 1–9, 2025.

[2] Mohsin, N. K. and D. K. Naji, "Design of a compact sub-6 GHz wideband filtering patch antenna without extra structure," *Progress In Electromagnetics Research C*, Vol. 155, 165–175, 2025.

[3] Kapoor, A., R. Mishra, and P. Kumar, "Wideband miniaturized patch radiator for sub-6 GHz 5G devices," *Heliyon*, Vol. 7, No. 9, 1–10, 2021.

[4] Sharma, M. D., A. Yadav, S. Singhal, and R. Sharma, "CPW fed textile UWB antenna for IoT and wearable applications," *Scientia Iranica*, 1–20, 2025.

[5] Katragadda, R. and P. A. N. Rao, "A compact CPW-fed textile-substrate-based half-circula spike monopole antenna," *Engineering Proceedings*, Vol. 59, No. 1, 149, 2023.

[6] Zhang, J., T. Chen, Y. Lv, and H. Xing, "A practical CPW-fed UWB antenna with reconfigurable dual band-notched characteristics," *Progress In Electromagnetics Research M*, Vol. 81, 117–126, 2019.

[7] Reha, A., O. Benkhadda, A. O. Said, A. E. Amri, and A. J. A. Al-Gburi, "Design of sub-6 GHz and sub-7 GHz dragon fractal antenna for 5G applications with enhanced bandwidth," *International Journal of Intelligent Engineering & Systems*, Vol. 18, No. 2, 14–22, 2025.

[8] Balanis, C. A., *Antenna Theory: Analysis and Design*, John Wiley & Sons, 2016.

[9] Khan, I., C. Song, H. Ullah, X. Qi, K. Zhang, S. Khan, Y. Shao, T. Gong, M. M. Kamal, M. Sheraz, and T. C. Chuah, "Investigation of coplanar waveguide fed SWB antenna with controllable stop band characteristics," *Scientific Reports*, Vol. 15, No. 1, 14051, 2025.

[10] Azim, R., R. Aktar, A. K. M. M. H. Siddique, L. C. Paul, and M. T. Islam, "Circular patch planar ultra-wideband antenna for 5G sub-6 GHz wireless communication applications," *Journal of Optoelectronics and Advanced Materials*, Vol. 23, No. 3–4, 127–133, 2021.

[11] Mudda, S., K. M. Gayathri, and M. Mallikarjun, "Wide-band frequency tunable antenna for 4G, 5G/sub 6 GHz portable devices and MIMO applications," *Progress In Electromagnetics Research C*, Vol. 118, 25–41, 2022.

[12] Nyami, G. N., O. Sokunbi, and A. A. Kishk, "Conformal ultra-wideband antenna for 5G-sub-6 GHz application," in *2024 IEEE International Symposium on Antennas and Propagation and INC/USNC-URSI Radio Science Meeting (AP-S/INC-USNC-URSI)*, 1615–1616, Firenze, Italy, 2024.

[13] Paul, L. C., H. K. Saha, T. Rani, M. Z. Mahmud, T. K. Roy, and W.-S. Lee, "An omni-directional wideband patch antenna with parasitic elements for sub-6 GHz band applications," *International Journal of Antennas and Propagation*, Vol. 2022, No. 1, 9645280, 2022.

[14] Lambert, U. M., U. K. Michael, and O. A. Bernard, "Ultra-wideband metamaterial-based rectangular microstrip antenna for sub-6 GHz 5G and other microwave applications," *Journal of Engineering Research and Reports*, Vol. 25, No. 7, 1–10, 2023.

[15] Alwareth, H., I. M. Ibrahim, Z. Zakaria, A. J. A. Al-Gburi, S. Ahmed, and Z. A. Nasser, "A wideband high-gain microstrip array antenna integrated with frequency-selective surface for sub-6 GHz 5G applications," *Micromachines*, Vol. 13, No. 8, 1215, 2022.

[16] Khandekar, R. and D. Sipal, "Sub-6 GHz ultrawideband gain enhanced antenna for IoT applications," *Arabian Journal for Science and Engineering*, 1–12, 2025.

[17] Megahed, A. A., M. Abdelazim, E. H. Abdelhay, and H. Y. M. Soliman, "Sub-6 GHz highly isolated wideband MIMO antenna arrays," *IEEE Access*, Vol. 10, 19 875–19 889, 2022.

[18] Tütüncü, B. and M. Kösem, "Substrate analysis on the design of wide-band antenna for sub-6 GHz 5G communication," *Wireless Personal Communications*, Vol. 125, No. 2, 1523–1535, 2022.

[19] Mahfuz, M. M. H., M. R. Islam, M. H. Habaebi, and J. Chebil, "Design of wearable textile patch antenna using C-shape etching slot," *International Journal of Interactive Mobile Technologies (iJIM)*, Vol. 16, No. 11, 107–120, 2022.

[20] Mandal, A., S. Sen, and T. Moyra, "Design of coplanar waveguide LPFs using open stub and defected ground structure (DGS)," *International Journal of Computational Intelligence & IoT*, Vol. 2, No. 3, 1–5, 2019.

[21] Li, L., X.-J. Dang, B. Li, and C.-H. Liang, "Analysis and design of waveguide slot antenna array integrated with electromagnetic band-gap structures," *IEEE Antennas and Wireless Propagation Letters*, Vol. 5, 111–115, 2006.

[22] Annam, K., S. K. Khah, S. Dooley, C. Cerny, and G. Subramanyam, "Experimental design of bandstop filters based on unconventional defected ground structures," *Microwave and Optical Technology Letters*, Vol. 58, No. 12, 2969–2973, 2016.

[23] Annam, K., "Design of bandstop filters using defected ground structures," Master's Thesis, University of Dayton, Dayton, OH, USA, 2015.

[24] Annam, K., B. Alemayehu, E. Shin, and G. Subramanyam, "Tunable filters using defected ground structures at millimeter-wave frequencies," *Micromachines*, Vol. 16, No. 1, 60, 2025.

[25] Santhakumar, G. and R. Muthukumar, "A novel compact flower shaped antenna array for sub-6 GHz and UWB applications," *Wireless Networks*, Vol. 31, No. 3, 2925–2938, 2025.

[26] Naik, D. K., A. K. Sahu, R. K. Parida, P. Raiguru, D. C. Panda, and R. K. Mishra, "Design of a broadband U-slot loaded E-shaped patch antenna using characteristic mode analysis," *AEU-International Journal of Electronics and Communications*, Vol. 154, 1–10, 2022.

[27] Chandan, , T. Srivastava, and B. S. Rai, "Multiband monopole U-slot patch antenna with truncated ground plane," *Microwave and Optical Technology Letters*, Vol. 58, No. 8, 1949–1952, 2016.

[28] Ansari, J. A. and R. B. Ram, "Analysis of broad band U-slot microstrip patch antenna," *Microwave and Optical Technology Letters*, Vol. 50, No. 4, 1069–1073, 2008.

[29] Bhobe, A. U., C. L. Holloway, M. Piket-May, and R. Hall, "Wide-band slot antennas with CPW feed lines: Hybrid and log-periodic designs," *IEEE Transactions on Antennas and Propagation*, Vol. 52, No. 10, 2545–2554, 2004.

[30] Xue, Y., R. Yan, W. Huang, and Y. Dong, "A wideband CPW slot antenna by using conductor-backed coplanar feeding," *Heliyon*, Vol. 10, No. 24, e40628, 2024.

[31] Dastranj, A. and M. Biguesh, "Broadband coplanar waveguide-fed wide-slot antenna," *Progress In Electromagnetics Research C*, Vol. 15, 89–101, 2010.